

Tuning the persistence lengths of main chain towards colorless and transparent polyimide with low dielectric loss and excellent general properties

Yitian Qin¹, Qian Yin¹, Junwei Lyu¹, Xu Wang^{**}, Xiangyang Liu^{*}

State key laboratory of polymer material and engineering, College of polymer science and engineering, Sichuan University, Chengdu, 610065, PR China

ARTICLE INFO

Keywords:

Colorless and transparent polyimide
Persistence length
Low dielectric loss

ABSTRACT

Colorless transparent polyimide (CPI) film simultaneously combining with low dielectric loss at high frequency, excellent thermal, mechanical properties and folding resistance is urgently required in nowadays flexible electronics industry. Inspired by liquid-crystal elastomers containing both soft and hard segments, one rigid and flexible single block copolymerization strategy was designed by introducing the hard segments of liquid-crystal-like PI into the flexible perfluorinated CPI, where it was found that tuning the persistence lengths of hard segments of liquid-crystal-like PI can significantly improve the general properties of CPI films. With the persistence lengths of main chain of CPI films increased from $2.17 \pm 0.07 \text{ \AA}$ to $16.56 \pm 0.12 \text{ \AA}$, the transmittance of CPI films at 550 nm remained above 85%, while the dielectric loss at 10 GHz of CPI films reduced from 0.00479 to 0.00407 with decrease of 15.1% due to the increased chain rigidity limits friction work. Besides, CPI film with the persistence length of $16.56 \pm 0.12 \text{ \AA}$ also exhibited well mechanical properties like thermal expansion coefficients of 24.8 ppm/K, tensile strengths of 162.5 MPa and Young's moduli of 4.88 GPa, which were 30.1%, 25.8% and 49.7% better than that of the CPI film with the persistence length of $2.17 \pm 0.07 \text{ \AA}$. Furthermore, this type of CPI films with tunable elasticity also had better folding resistance properties. Therefore, tuning the persistence lengths of main chain of CPI films can meet the application of high frequency/speed communication, flexible display and other fields at the same time.

1. Introduction

Nowadays, colorless transparent polyimides (CPIs) with light weight, high transparency, flexibility and excellent thermal resistance properties are widely used in fields of polymer substrate, flexible displays and electrodes, which seems like the most suitable choice to replace traditional rigid inorganic substrates [1,2]. With the further development of polymer substrate applied in flexible displays and flexible electrodes, new challenges containing low D_k and D_f at high frequency, unlimited coefficient of thermal expansion (CTE) and excellent mechanical properties started to appear in the design of CPIs [3].

Classical method for manufacturing CPI films with high transparency was mostly considered from inhibiting formation of intermolecular charge transfer complexes (CTCs), including introduce a large number of strong electronegative groups (such as fluorine-containing groups) [4–7], pendant groups [8–10], alicyclic structures [11–19],

non-coplanar and twisted structures [20–23], while these methods will seriously disturb the linearity and rigidity of polyimide molecular chain, which further weaken the intermolecular force of CPI as consistent result of poor CTC, and finally weakened the thermal, mechanical and folding-resistant properties of CPI while improving transparency. For example, Yan et al. designed and synthesized type of novel rigid, twisted and non-coplanar alicyclic dianhydride monomers and semi-alicyclic diamine monomers, which inhibited the accumulation of molecular chains, destroyed the conjugation of the main chain, and hindered the formation of intermolecular charge transfer complexes, thereby preparing CPI films with not bad optical properties ($T_{400} > 78\%$). However, due to the lack of structural stiffness, the T_g and CTE were often insufficient for practical applications [22]. Therefore, according to the practical research and application of CPIs in this field, it was gradually found that there was almost no way to raise effective strategy to indeed balance above strategies and simultaneously make them well, and this

* Corresponding author.

** Corresponding author.

E-mail addresses: wangxu@scu.edu.cn (X. Wang), lxy@scu.edu.cn (X. Liu).

difficulty was actually reflected from some intrinsic conflicts inside molecular mechanisms of CPIs.

In recent years, the introduction of a large number of hydrogen bonds and coordination effects to enhance intermolecular forces not only maintained high transparency, but also significantly improved the mechanical properties and reduced the CTE of CPI films [24–28]. For example, Ahn et al. constructed hydrogen bond-coordination bond double network by introducing amide linkage and Li^+ , the elastic moduli of CPI film increased by 42.37%, the average transmittance of CPI film in the range of 400–800 nm was around 90%. Besides, it can be folded by over 200,000 times without creases at a fold radius of 3 mm. However, because of the introduction of much amide linkage with high polarity, this method was difficult to further reduce the D_k and D_f of CPI films [29]. Moreover, Chen et al. prepared a cellulose nanocrystal (CNC)/CPI hybrid substrate with high optical, mechanical, and thermal properties, but strategy as blending is difficult to adjust filler dispersion and long-term interface stability, which was not suitable for engineering [30]. Therefore, how to prepare CPI films with intrinsic high transparency, low dielectric loss at high frequency, good folding resistance and excellent mechanical properties, which can meet the application in high frequency and high speed communication, flexible display and other fields at the same time is an industry problem.

In our previous study, homopolymerization of p-phenylene bis(trimellitate) dianhydride (TAHQ) with rigid mesogen (aromatic ester groups) and 2,2'-bis-(trifluoromethyl)benzidine (TFMB) with $-\text{CF}_3$ had been proved to be an effective hard segment to induce liquid crystal-like behavior in whole polyimide chain, which dramatically reduced the D_f at high frequency and enhanced the mechanical properties of liquid crystal-like PI film. However, due to the high crystallinity, TAHQ-TFMB showed opacity that was not conducive to application in fields of polymer substrate, flexible displays and flexible electrodes [31].

In this article, based on the classical CPI structure system with excellent colorless and transparency, 4,4'-hexafluoroisopropenyl diphthalic anhydride-TFMB (6FDA-TFMB), a universal algorithm for revealing persistence length of CPI was first derived to establish, which was considered as typical representation for depicting chain elasticity of CPI. Moreover, copolymerization modification of 6FDA-TFMB structure system was carried out by using liquid crystal-like hard segment, and one controllable polymerization method was used to regulate the aggregation situation of TAHQ in the main chain, where firstly obtained amino-terminated liquid crystal-like oligomers with various degree of polymerization and then a certain amount of 6FDA was added to obtain CPI films with various persistence lengths. It was found that with the persistence lengths of CPI films increased from $2.17 \pm 0.07 \text{ \AA}$ to $16.56 \pm 0.12 \text{ \AA}$, the transmittance of CPI films at 550 nm remained above 85%, and the D_f at 10 GHz of CPI films reduced from 0.00479 to 0.00407 with decrease of 15.1%. Besides, the CPI film with the persistence length of $16.56 \pm 0.12 \text{ \AA}$ exhibited thermal expansion coefficients of 24.8 ppm/K, tensile strengths of 162.5 MPa and Young's moduli of 4.88 GPa, which were 30.1%, 25.8% and 49.7% better than that of the CPI film

with the persistence length of $2.17 \pm 0.07 \text{ \AA}$. Furthermore, the CPI films also had better folding resistance properties. Therefore, tuning the persistence lengths of CPI films can meet the application of high frequency/speed communication, flexible display and other fields at the same time, which vigorously promote the development of these fields.

2. Experimental SECTION

2.1. Synthesis of random copolymer PAA with various TAHQ content

As shown in Fig. 1(a), in order to ensure the random distribution of the two anhydrides, p-phenylene-bis (tricarboxylate) dianhydride (TAHQ) and 4,4'-hexafluoroisopropenyl diphthalic anhydride (6FDA) were first weighed and dispersed in the solvent DMAc at a molar ratio of 60:40, and then 2,2'-bis (trifluoromethyl) benzidine (TFMB) with the same total molar number of the two dianhydrides was added. Then, viscous PAA solution was obtained after reaction for 10 h in argon atmosphere. The obtained PAA was named TAHQ-60-r, according to the TAHQ content.

2.2. Controllable polymerization of single block copolymer PAA with various DP of liquid-crystal-like segments

As shown in Fig. 1(b), firstly, TAHQ and TFMB with a certain molar ratio were added to DMAc, and the amino-terminated liquid-crystal-like oligomer was obtained after reaction at room temperature for 3 h. The relationship between the degree of polymerization (DP) of the oligomer and the molar ratio of the monomer satisfied formula (1) to (2):

$$DP = \frac{1}{1 - p} \quad (1)$$

$$p = \frac{n_{TAHQ}}{n_{TFMB}} \quad (2)$$

Among them, p , n_{TAHQ} , n_{6FDA} and n_{TFMB} were the degree of monomer reaction, the molar number of anhydride groups in TAHQ, the molar number of anhydride groups in 6FDA and the molar number of amine groups in TFMB, respectively. After obtaining liquid crystal-like oligomers with various DP, a certain amount of 6FDA was added to the three-necked bottle to react with the terminal amino group of the liquid crystal-like oligomer, and the residual monomers were added to ensure the equal molar ratio of dianhydride to diamine in the system. After all of the monomer was added, the reaction was continued in argon atmosphere for 10 h.

2.3. Preparation of CPI films

The acid absorbent and catalyst for chemical imidization were added to the PAA solution as certain amount. After 10 h, according to Fig. S1, PI solution with the 0–5 DP of liquid crystal-like segments was colorless

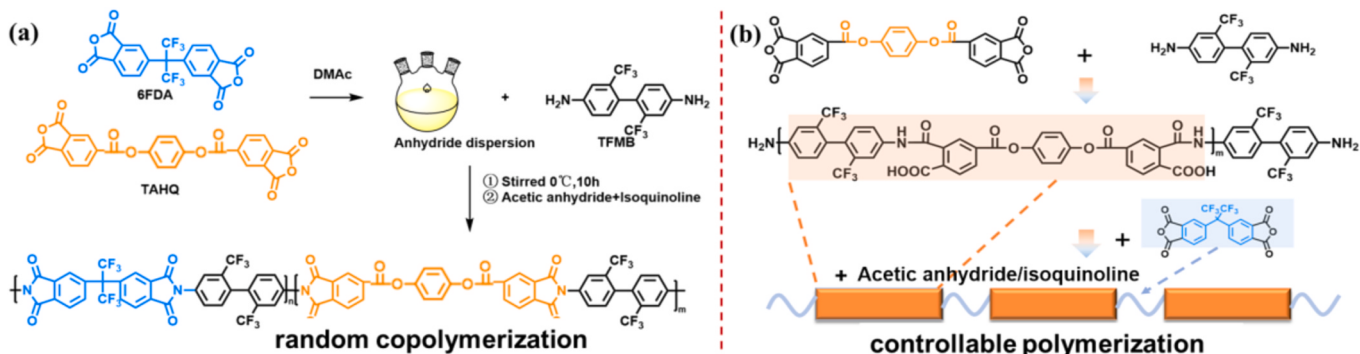


Fig. 1. (a) Synthetic route of random polymerization. (b) Synthetic route of controllable polymerization.

and transparent homogeneous solution with good solubility. However, when the DP of liquid crystal-like segment increased to 10, PI solution showed a white gel, indicating that the PI with DP of 10 of liquid crystal-like segment had poor solubility after chemical imidization and it was difficult to prepare CPI film by chemical imidization. Therefore, block copolymerization was used to prepare the CPI film with the DP of 10 of liquid crystal-like and flexible segments, which showing at Fig. S2.

After chemical imidization, the mixed solution was precipitated with ethanol to obtain PI filaments. The PI filaments were dissolved with DMAc to prepare PI solution, and then the PI solution was evenly coated on a flat and clean glass plate with an automatic coating machine. Then the substrate coated with PI solution was vacuum dried at 90 °C for 2 h, and then annealed at 300 °C for 0.5 h to obtain CPI film. According to the TAHQ content, the copolymerization method and the DP of segments, the obtained CPI films were named TAHQ-60-X0 (random co-CPI), TAHQ-60-X1, TAHQ-60-X3, TAHQ-60-X5, TAHQ-60-X10.

3. RESULTS and DISCUSSION

3.1. Confirmation of sequence structure and algorithm of persistence lengths of CPI films

In order to characterize the sequence structure of the liquid-crystal-like segment of CPI films, firstly, infrared spectrum in Fig. 2(a) contains 6FDA-TFMB, TAHQ-TFMB, TAHQ-60-X0, TAHQ-60-X1, TAHQ-60-X3, TAHQ-60-X5, TAHQ-60-X10 supported the effective adjustment in their sequential structure. For the PI films containing TAHQ, the characteristic absorption peaks of aromatic ester groups appeared at 1737 cm⁻¹ and 1280 cm⁻¹ [32,33]. The changes of ester characteristic absorption peaks (1280 cm⁻¹) in PI films were compared in Fig. 2(b). It can be seen from the diagram that as the DP of the liquid-crystal-like segments in PI films increased from 0 to 5, the peak height of PI films at 1280 cm⁻¹ gradually increased. After calculated, the peak intensities of TAHQ-0

(6FDA-TFMB), TAHQ-60-X0, TAHQ-60-X1, TAHQ-60-X3, TAHQ-60-X5, TAHQ-60-X10, and TAHQ-100 (TAHQ-TFMB) were 0, 0.001, 0.005, 0.009, 0.012, 0.011, and 0.019, respectively, increasing with the increase of the DP of liquid-crystal-like segments.

Nuclear magnetic resonance spectroscopy is considered to characterize the sequence structure of polymers more precisely. Fig. 2(c) was the 1H NMR spectra of PAA with various sequence structures. Peaks of COOH and CO-NH on the main chain of PAA can be clearly seen near 13.65 ppm and 10.96 ppm [33]. In addition, after amplifying the peak of PAA amide H (Fig. 2(d)), it can be seen that there were two obvious peaks of amide NH of PAA, which were located near 10.98 ppm and 10.95 ppm, respectively, and the integral area ratio of the two peaks was roughly 2:3, indicating that the two peaks at 10.98 ppm and 10.95 ppm corresponded to the amide NH between 6FDA-TFMB and TAHQ-TFMB, respectively. Therefore, the NMR spectra of PAA with various sequence structures were deconvoluted as shown in Fig. 2(e) and Fig. S4 [34]. As the results shown in Fig. 2(f) and Table S1, it can be obviously seen that the area percentage of TA-TF-TA amide bond in TAHQ-60-X1, TAHQ-60-X3, TAHQ-60-X5 and TAHQ-60-X10 increased with the increase of DP. In summary, these results still proved that the CPI films with various sequence structures were successfully synthesized by the controllable polymerization method.

Persistence length of polymer is induced to depict stiffness of above synthesized polymer chains which is usually measured by the light scattering experiment of polymer dilute solution. The theoretical methods of studying persistence length include worm-like chain model and the transformation matrix method with the help of the concept of virtual key [35–42]. Otherwise, in this article, the persistence length of a polymer chain was studied from its definition. As shown in eq. (3), persistence length (P) is the average sum of the projections of all bonds $j \geq i$ on bond i in an infinitely long chain [43].

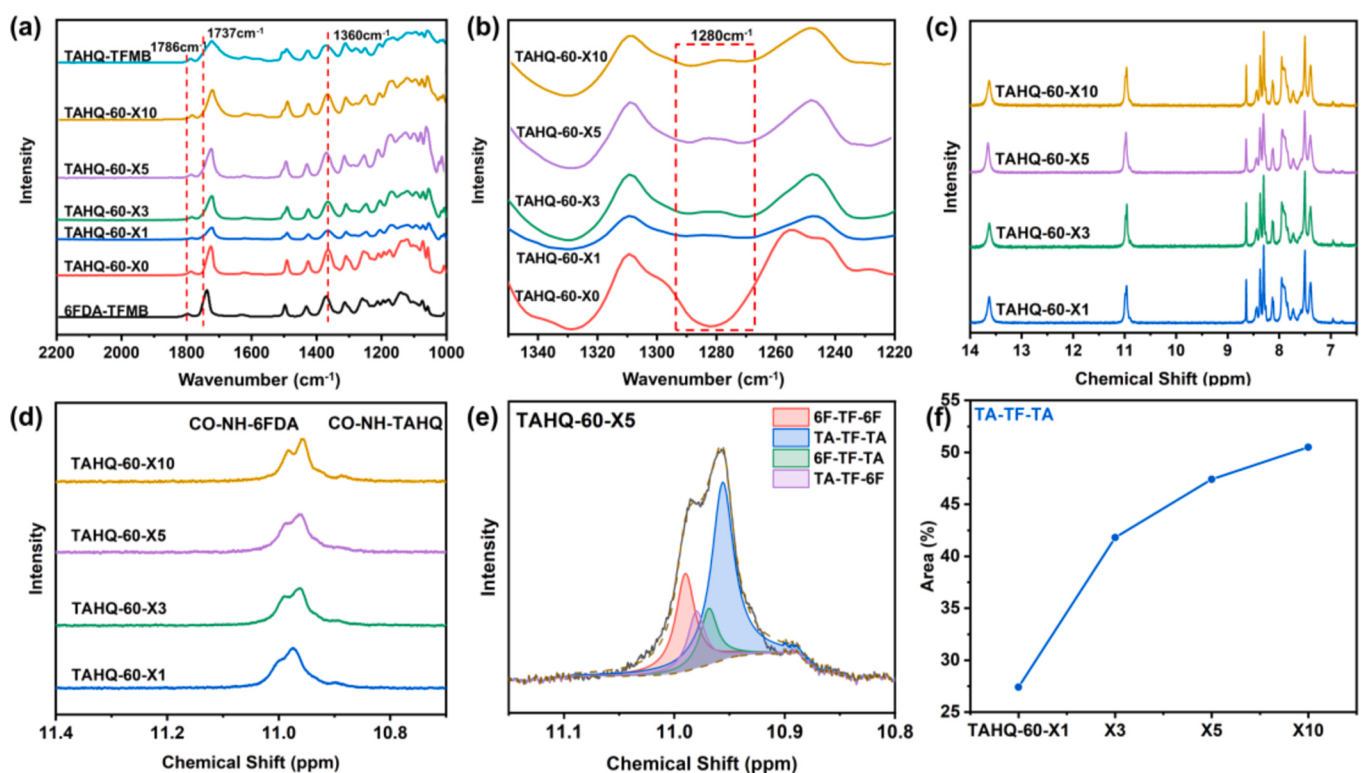


Fig. 2. (a) FTIR spectra of various CPI films, (b) zooming of FTIR spectra of various CPI films, (c) NMR-H¹ spectra of PAA with various sequence structure, (d) zooming of NMR-H¹ spectra of PAA with various sequence structure, (e) –NH in TAHQ-60-X5 PAA, (f) Area ratio of amide bonds assigned to TA-TF-TA among PAA with various sequence structure.

$$P_i = \frac{\mathbf{b}_i \bullet \mathbf{R}_{ij}}{|\mathbf{b}_i|} \Big|_{j \rightarrow \infty} \quad (3)$$

where \mathbf{b}_i is the i th bond vector, and $\mathbf{R}_{m,n}$ is the vector from the beginning of \mathbf{b}_m to the end of \mathbf{b}_n . If P is convergent when $i \rightarrow \infty$, then the long chain is non-rigid. At this time, it is easy to get $\langle P_1 \rangle = \langle P_i \rangle = P$.

In reality, the length of the polymer chain is limited. The vector from one end of the linear polymer to the other end is \mathbf{R} , and its length (R) is called the end distance. For a polymer chain with the n number of equal-length bonds in the main chain, the \mathbf{R} of the polymer chain was shown in eq. (4),

$$\mathbf{R} = \mathbf{b}_1 + \mathbf{b}_2 + \dots + \mathbf{b}_n = \sum_{i=1}^n \mathbf{b}_i \quad (4)$$

$$R^2 = \mathbf{R}^2 = \sum_{i=1}^n \mathbf{b}_i \bullet \sum_{j=1}^n \mathbf{b}_j = nb^2 + 2 \sum_{j>i} \mathbf{b}_i \bullet \mathbf{b}_j \quad (5)$$

If $n \rightarrow \infty$,

$$\sum_{j>i} \mathbf{b}_i \bullet \mathbf{b}_j = \mathbf{b}_i \bullet \mathbf{R}_{i+1,j} = bP_i - b \quad (6)$$

Among them, $b = |\mathbf{b}_i|$. Then substituting eq. (6) into eq. (5) will get mean square end-to-end distance of the polymer chain as shown in eq. (7). Furthermore, the persistence length of the polymer chain can be obtained with eq. (8).

$$\langle R^2 \rangle = nb^2 + 2b \sum_i (\langle P_i \rangle - b) = 2nbP - nb^2 \quad (7)$$

$$P = \frac{\langle R^2 \rangle}{2nb} + \frac{b}{2} \quad (8)$$

According to eq. (8), if the number of single keys of single chain (n), average single bond length of single chain (b) and mean square end-to-end distance of single chain ($\langle R^2 \rangle$) were obtained, the persistence lengths of PI chain will be acquired. For the purpose of evaluating persistence lengths, molecular simulation was used to provide a theoretical estimate of the persistence lengths of these CPI polymer chains. Firstly, TAHQ-60-X0, TAHQ-60-X1, TAHQ-60-X3, TAHQ-60-X5, and TAHQ-60-X10 were constructed with the same number of structural units but different sequence structures, meaning that the n and b of TAHQ-60-X0, TAHQ-60-X1, TAHQ-60-X3, TAHQ-60-X5, and TAHQ-60-X10 were the same value. According to the single chain models of molecular simulation, it can be easily got that $n = 740$, $b = 1.445 \text{ \AA}$, the mean square end-to-end distances ($\langle R^2 \rangle$) of TAHQ-60-X0, TAHQ-60-X1, TAHQ-60-X3, TAHQ-60-X5, and TAHQ-60-X10 were $3103.8 \pm 158.9 \text{ \AA}^2$, $11298.3 \pm 156.5 \text{ \AA}^2$, $22238.6 \pm 527.7 \text{ \AA}^2$, $33879.6 \pm 263.7 \text{ \AA}^2$, and $79724.4 \pm 7692.0 \text{ \AA}^2$, respectively [35]. Then substituting n , b and $\langle R^2 \rangle$ into eq. (8), the persistence lengths (P) of TAHQ-60-X0, TAHQ-60-X1, TAHQ-60-X3, TAHQ-60-X5, and TAHQ-60-X10 were $2.17 \pm 0.07 \text{ \AA}$, $6.01 \pm 0.07 \text{ \AA}$, $11.12 \pm 0.25 \text{ \AA}$, $16.56 \pm 0.12 \text{ \AA}$, and $39.69 \pm 1.22 \text{ \AA}$, respectively. According to the results, the CPI chains with various persistence lengths were successfully prepared by controllable polymerization. Besides, with the degree of polymerization (DP) of the liquid-crystal-like hard segments increased, the persistence lengths of CPI chains significantly increased from $2.17 \pm 0.07 \text{ \AA}$ to $39.69 \pm 1.22 \text{ \AA}$.

As shown in Fig. 3(c), the dichroic ratios of TAHQ-60-X0, TAHQ-60-X1, TAHQ-60-X3, TAHQ-60-X5, and TAHQ-60-X10 were 1.52, 2.02, 2.15, 2.2, and 3.03, respectively, indicating that the in-plane orientation of CPI films increased with the persistence lengths of CPI films [31]. Among all the CPI films, the orientation degree of TAHQ-60-X10 with the longest persistence length was 99.3% higher than that of TAHQ-60-X0 with the shortest persistence length, indicating that the

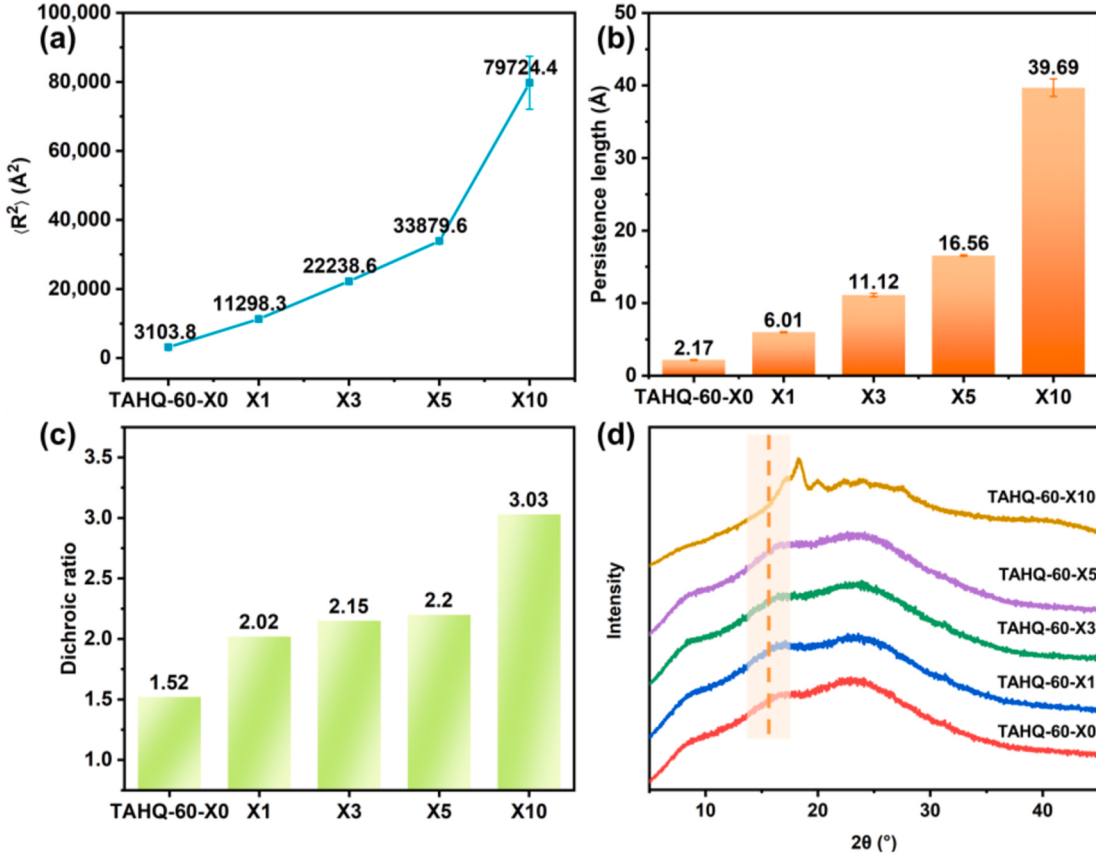


Fig. 3. (a) The mean square end-to-end distances of various CPI model molecules, (b) persistence lengths of various CPI films, (c) dichroic ratio of CPI films with various persistence lengths, (d) XRD patterns of CPI films with various persistence lengths.

longer persistence length of CPI films was more conducive to improve the in-plane orientation degree of CPI films.

It can also be seen from the XRD patterns of CPI films in Fig. 3(d) that as the persistence lengths of CPI films gradually increased, the diffraction peaks (near 18.3°) related to the orientation of the phenyl ester group gradually increased, indicating that the extension of the persistence lengths of CPI films increased the degree of chain order [44]. The results also showed that with the increasing persistence lengths of CPI films, the liquid crystal-like segments in the main chain of CPI films would also gradually enriched, simultaneously demonstrated that the CPI films with various persistence lengths were successfully prepared by the controllable polymerization method. Furthermore, TAHQ-60-X0, TAHQ-60-X1, TAHQ-60-X3 and TAHQ-60-X5 showed a large dispersion peak, presenting an amorphous state far away from liquid-crystal-like structure. However, two strong peaks of TAHQ-60-X10 respectively assigned to the (110) plane and (200) plane can be found at 18.3° and 22°, indicating that TAHQ-60-X10 with the longest persistence length was mostly aligned parallel to the film plane and had high crystallinity.

3.2. Optical properties of CPI films with various persistence lengths

The transparency of CPI films with various persistence lengths was

compared in Fig. 4(a), which can be seen that the UV-vis curves of TAHQ-60-X0, TAHQ-60-X1, TAHQ-60-X3 and TAHQ-60-X5 were basically coincident, while the UV-vis curve of TAHQ-60-X10 was lower. In Fig. 4(b), the transmittance of CPI films at 550 nm was calculated. The transmittance of TAHQ-60-X0, TAHQ-60-X1, TAHQ-60-X3, TAHQ-60-X5 and TAHQ-60-X10 at 550 nm were 85.6%, 85.6%, 85.2%, 86.0%, and 81.7%, respectively, indicating that the persistence lengths of CPI films which in the range of $2.17 \pm 0.07 \text{ \AA}$ ~ $16.56 \pm 0.12 \text{ \AA}$ almost no impacted the transmittance of TAHQ-60-X0, TAHQ-60-X1, TAHQ-60-X3 and TAHQ-60-X5. However, when the persistence lengths of TAHQ-60-X10 increased to $39.69 \pm 1.22 \text{ \AA}$, the stronger linearity and stiffness caused the higher in-plane orientation degree and crystallinity, further causing that the transmittance at 550 nm of TAHQ-60-X10 was only 81.7%, which cannot be used as colorless and transparent polyimide. Therefore, the other properties of TAHQ-60-X10 will be not discussed anymore.

3.3. Limited chain polarization and friction under wide-range of electromagnetic field promoted low D_k/D_f

Since the persistence lengths of CPI films had been proved to significantly affect the stiffness and orientation of CPI films, Fig. 4(c-i) and Table S2 compared the dielectric properties at 10 GHz of CPI films

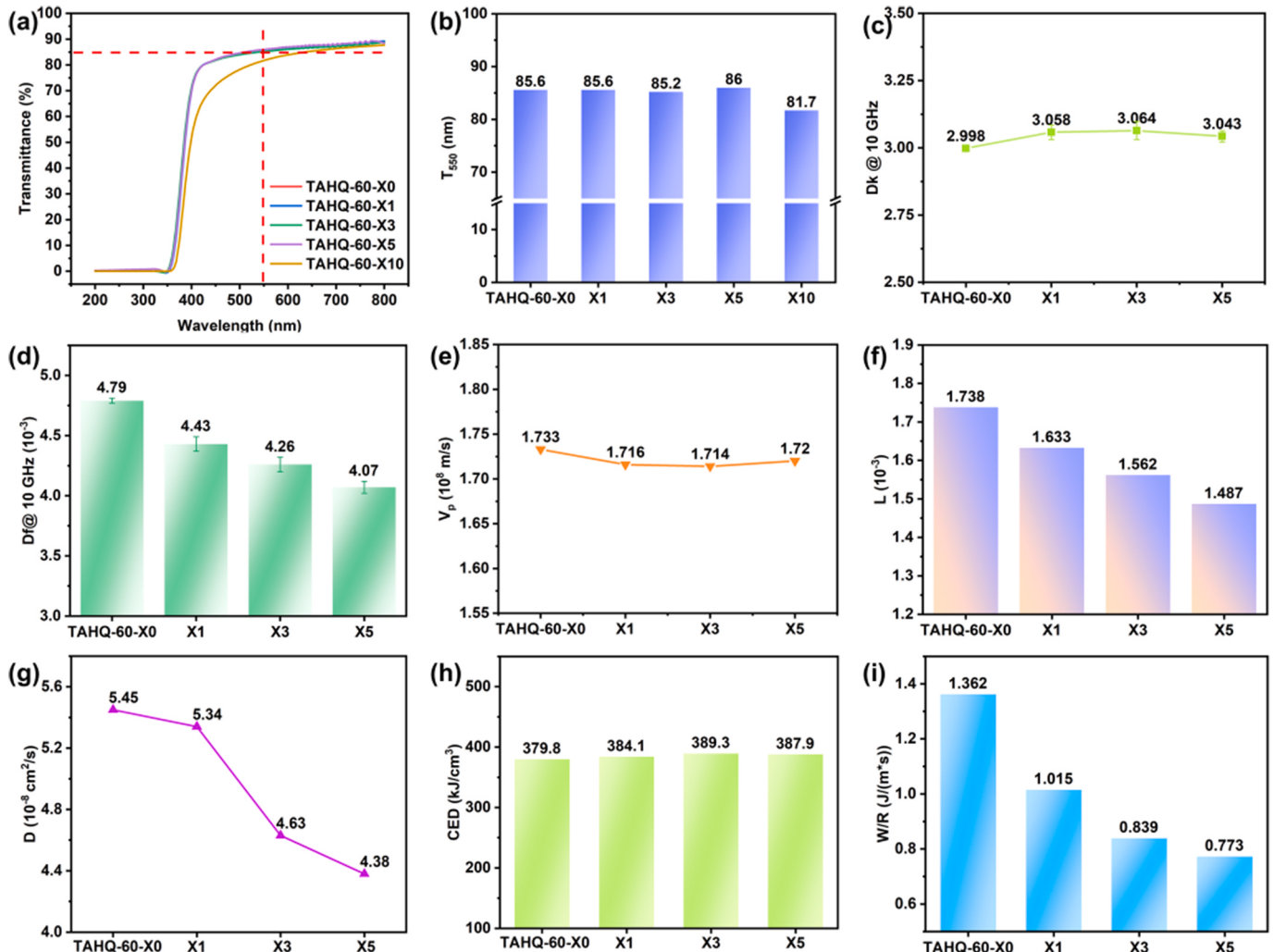


Fig. 4. (a) UV-vis curves of CPI films with various sequence structure. (b) Transmittance at 450 nm of CPI films with various sequence structure. (c) $D_k @ 10 \text{ GHz}$ of CPI films with various sequence structure. (d) $D_f @ 10 \text{ GHz}$ of CPI films with various sequence structure. (e) $V_p @ 10 \text{ GHz}$ of CPI films with various sequence structure. (f) $L @ 10 \text{ GHz}$ of CPI films with various sequence structure. (g) Diffusion coefficient of various PI models with frequency of 10 GHz. (h) CED of various CPI models. (i) Frictional work of various PI models corrected by dichroic ratio with with frequency of 10 GHz.

with various persistence lengths. As shown in Fig. 4(c), due to the low polarizability and high free volume of backbone chains, the dielectric constant (D_k) of TAHQ-60-X0, TAHQ-60-X1, TAHQ-60-X3 and TAHQ-60-X5 at 10 GHz were 2.998 ± 0.005 , 3.058 ± 0.027 , 3.064 ± 0.033 and 3.043 ± 0.021 , respectively, which increased slightly with the persistence lengths of CPI films, indicating that the persistence lengths of CPI films had little effect on the D_k at 10 GHz of CPI films. Different from the change of D_k , the dielectric loss (D_f) of CPI films with various persistence lengths at 10 GHz decreased rapidly with the increase of persistence lengths of CPI films. As shown in Fig. 4(d), the D_f of TAHQ-60-X0, TAHQ-60-X1, TAHQ-60-X3 and TAHQ-60-X5 at 10 GHz were 0.00479 ± 0.00002 , 0.00443 ± 0.00006 , 0.00426 ± 0.00006 and 0.00407 ± 0.00005 , respectively. Among them, the D_f of TAHQ-60-X5 was 15.1% lower than that of TAHQ-60-X0 at 10 GHz.

It was discovered that the D_k and D_f of CPI films at 10 GHz were actually oriented to their transmission rate and transmission loss in high-frequency communication applications. Therefore, as shown in eq. (9) and eq. (10), based on the relationship between signal transmission rate (V_p) and signal transmission loss (L) at high frequency and the D_k , D_f of PI, the transmission rate (V_p) and transmission loss (L) of the copolymer PI films with various sequence structures at 10 GHz were also calculated in Fig. 4(e-f) and Table S2:

$$V_p = \frac{C}{\sqrt{D_k}} \quad (9)$$

$$L = \frac{f}{C} \times D_f \times \sqrt{D_k} \quad (10)$$

where C is the speed of light and f is the external frequency. As shown in Fig. 4(g), the V_p of TAHQ-60-X0, TAHQ-60-X1, TAHQ-60-X3 and TAHQ-60-X5 at 10 GHz were 1.733×10^8 m/s, 1.716×10^8 m/s, 1.714×10^8 m/s and 1.720×10^8 m/s, respectively. In addition, the transmission loss of CPI films with various persistence lengths showed a similar variation with D_f . As shown in Fig. 4(f), the L of TAHQ-60-X0, TAHQ-60-X1, TAHQ-60-X3 and TAHQ-60-X5 at 10 GHz were 1.738×10^{-3} , 1.633×10^{-3} , 1.562×10^{-3} and 1.487×10^{-3} , respectively, which decreased rapidly with the increase of persistence lengths of CPI films. Among them, the transmission loss of TAHQ-60-X5 with the longest persistence length was 12.8% smaller than that of TAHQ-60-X0, indicating that extending the persistence lengths of CPI films, high crystallinity and stiffness can effectively reduce the L and D_f of the CPI films at 10 GHz during high frequency transmission.

In order to further understand the mechanism of how persistence lengths of CPI films affecting the D_f of CPI films at 10 GHz, dielectric behavior at 10 GHz of above CPI films with various persistence lengths were investigated by molecular dynamics simulation. Based on the CPI model construction, an 10 GHz electric field with was applied to the CPI model according to the method shown in Support Information. Eq. S4 in Supporting Information revealed, diffusion coefficients (D) of TAHQ-60-X0, TAHQ-60-X1, TAHQ-60-X3 and TAHQ-60-X5 at 10 GHz performed as 5.45×10^{-8} cm²/s, 5.34×10^{-8} cm²/s, 4.63×10^{-8} cm²/s, and 4.38×10^{-8} cm²/s, respectively in Fig. 4 (g), indicating that the long persistence lengths effectively slowed down the rate of polarization of CPI at 10 GHz, which simultaneously reduced the polarization friction work of CPI at 10 GHz [45]. According to our previous study, the polarization friction work of polymer chains was strongly associated with D_f , that dipoles in PI rotating under electric fields were simultaneously affected by friction and electric field forces [31]. Therefore, the dielectric loss was caused by intermolecular friction work, which was determined by the friction and displacement [46–48]. The corrected polarization friction work of the above PI models with various persistence lengths was calculated based on the friction work calculation formula [31].

$$W / R = A' \times CED \times D/R \quad (11)$$

According to eq. (11), the cohesive energy densities (CED) of different PI models was resolved, where related results were exhibited in Fig. 4(h). The CED of TAHQ-60-X0, TAHQ-60-X1, TAHQ-60-X3 and TAHQ-60-X5 were 379.8 kJ/cm³, 384.1 kJ/cm³, 389.3 kJ/cm³ and 387.9 kJ/cm³, respectively, indicating that the persistence length had little influence on the intermolecular friction of CPI [49]. Based on the previously calculated R, CED and D, the corrected polarization friction work of the above different PI models was calculated. Results showed in Fig. 4(i) and Table S3 revealed that the corrected polarization friction work of TAHQ-60-X0, TAHQ-60-X1, TAHQ-60-X3 and TAHQ-60-X5 were respectively 1.362 J/(m × s), 1.015 J/(m × s), 0.839 J/(m × s) and 0.773 J/(m × s), indicating a downward trend with the improvement of persistence length, which was as the same trend as the change of D_f in Fig. 4(d). The results proved that the introduction of long persistence lengths can effectively increased the stiffness and reduce the polarization friction work of CPI at 10 GHz by slowing down the polarization motion rate, thereby reducing the dielectric loss of CPI at 10 GHz.

3.4. Enhanced chain rigidity delayed CPIs relaxation during thermal shock

According to Fig. 5(a) and (c), it can be observed that the Tan Delta curve of Dynamic Mechanical Analysis (DMA) of the films exhibited α and β transitions, which probably corresponding to glass transition and rotation-related relaxation process [33,50,51]. The peak temperature in the tan δ curves was regarded as the glass transition temperature (T_g) of CPI films. The T_{gs} of TAHQ-60-X0, TAHQ-60-X1, TAHQ-60-X3 and TAHQ-60-X5 were 330.1 °C, 338.4 °C, 336.1 °C and 336.3 °C, indicating that the extension of persistence lengths of CPI films did not significantly affect T_g of CPI films. However, the height of α transition peak of TAHQ-60-X0, TAHQ-60-X1, TAHQ-60-X3 and TAHQ-60-X5 were 0.595, 0.524, 0.501 and 0.460. According to the height of α transition peak, liquid crystal-like hard segments visible restricted the motion of the chain segments, and the extension of persistence lengths of CPI films was beneficial to the thermal properties of CPI films.

The thermal dimensional stability of CPI films in the range of 40–250 °C were showing in Fig. 5(b) and (c). And the coefficient of thermal expansion (CTE) of TAHQ-60-X0, TAHQ-60-X1, TAHQ-60-X3 and TAHQ-60-X5 were 35.5 ppm/K, 27.7 ppm/K, 26.5 ppm/K and 24.8 ppm/K. Among them, the CTE of TAHQ-60-X5 was 30.1% lower than that of TAHQ-60-X0, indicating that with the extension of persistence lengths of CPI films, high degree of orientation and stiffness can greatly increase the thermal dimensional stabilities and decrease the CTE of CPI films [50].

3.5. Enhanced chain rigidity delayed CPIs relaxation during tensile progress

As shown in Fig. 6(a) and Table S4, the tensile strength of TAHQ-60-X0, TAHQ-60-X1, TAHQ-60-X3 and TAHQ-60-X5 was 129.2 ± 0.7 MPa, 147.1 ± 7.0 MPa, 153.5 ± 0.4 MPa and 162.5 ± 6.9 MPa, respectively. The Young's modulus of TAHQ-60-X0, TAHQ-60-X1, TAHQ-60-X3 and TAHQ-60-X5 was 3.26 ± 0.04 GPa, 4.24 ± 0.11 GPa, 4.82 ± 0.04 GPa and 4.88 ± 0.31 GPa, respectively. Among them, the tensile strength and Young's modulus of TAHQ-60-X5 were 25.8% and 49.7% higher than that of TAHQ-60-X0. Therefore, the mechanical properties of CPI films showed that the long persistence length of CPI films with high degree of orientation and stiffness can effectively improve the tensile strength and Young's modulus of CPI films.

3.6. Elastic deformation range and folding resistance of CPI films with various persistence lengths

The CPI films with excellent transmittance, low dielectric loss at 10 GHz, outstanding thermal and mechanical properties were successfully

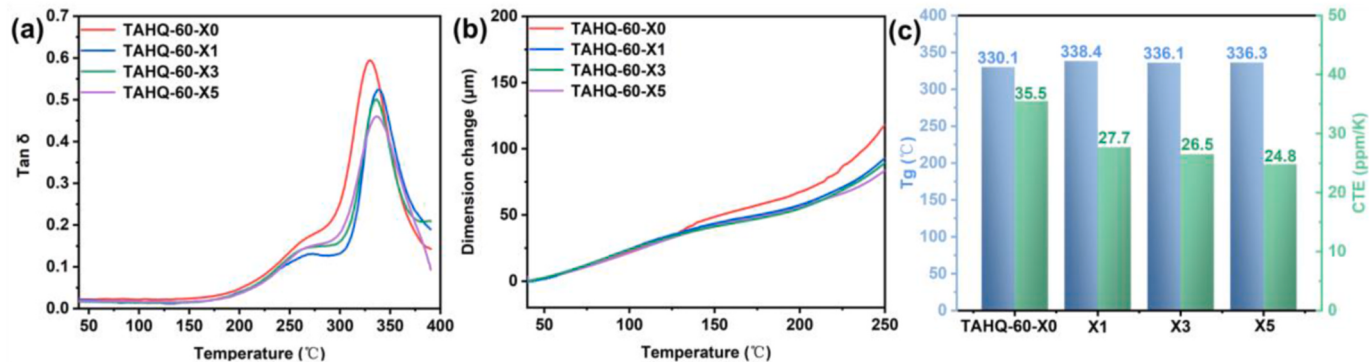


Fig. 5. (a) Tan Delta curves of CPI films with various persistence lengths. (b) Dimensional changes of CPI films with various persistence lengths ranging from 40 to 250 °C. (c) Tg and CTE values of CPI films with various persistence lengths.

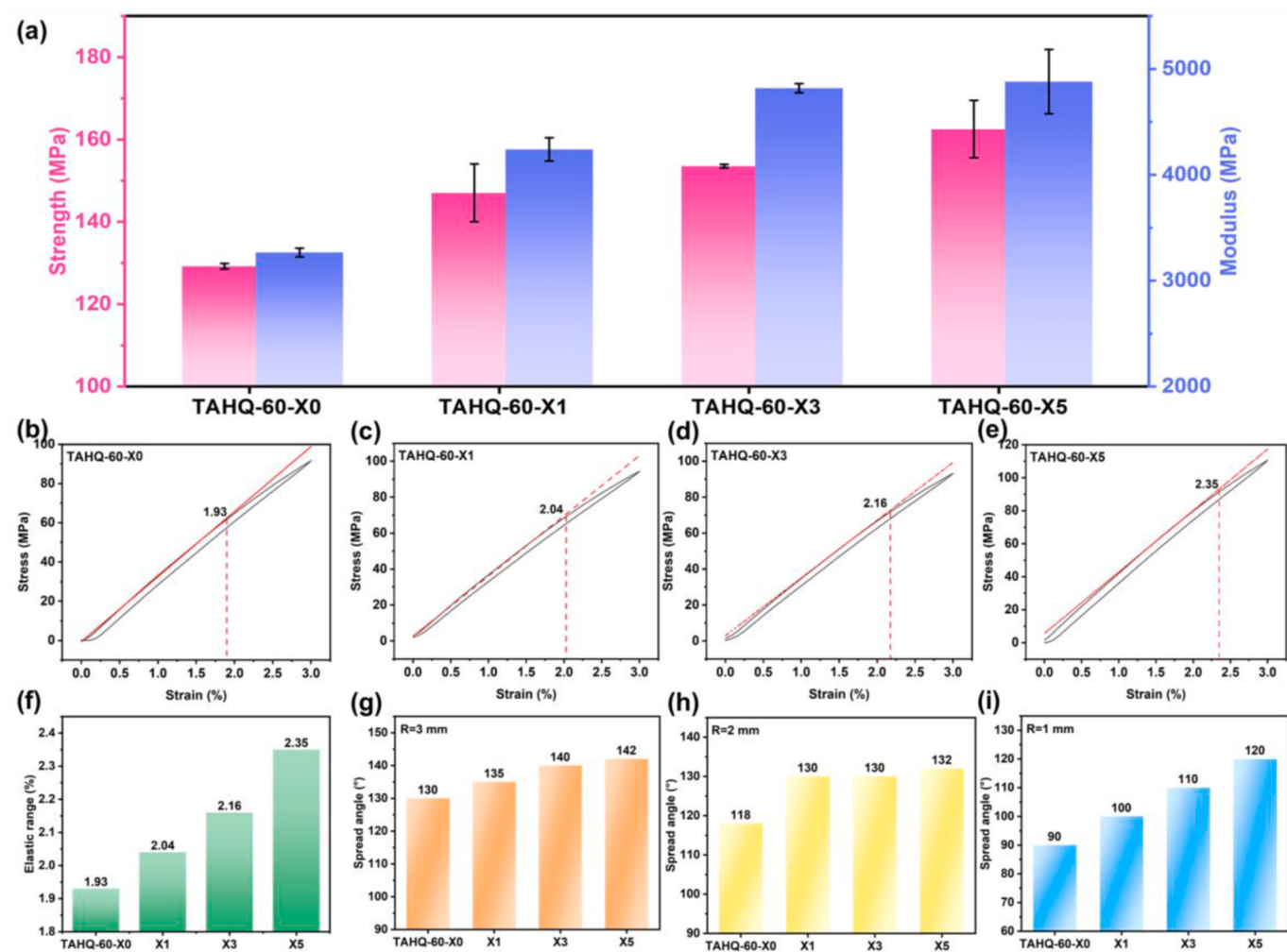


Fig. 6. (a) Mechanical properties of PI films with various persistence lengths. Stress-strain curves of (b) TAHQ-60-X0 films, (c) TAHQ-60-X1 films, (d) TAHQ-60-X3 films, (e) TAHQ-60-X5 films. (f) Elastic range of CPI films with various persistence lengths. Spread angles of various CPI films under curvature radius of (g) 3 mm, (h) 2 mm, (i) 1 mm.

prepared through tuning persistence lengths of CPI films. With the rapid development of flexible electronics and high frequency communication technology, the folding-resistant CPI films were becoming more and more important [20,29,52–55]. Based on the formation of creases, in our previous study, a new idea was proposed to improve the folding resistance by expanding the elastic deformation range of PI films, in order to

ensure that the strain did not exceed the elastic deformation range during folding and prevent the accumulation of plastic deformation [56]. Therefore, in Fig. 6(b–e), the elastic deformation intervals of CPI films with various persistence lengths were calculated. The elastic deformation ranges of TAHQ-60-X0, TAHQ-60-X1, TAHQ-60-X3 and TAHQ-60-X5 were 1.93%, 2.04%, 2.16% and 2.35%, respectively,

showing a trend of increasing with the increase of persistence lengths of CPI films. The elastic deformation range of TAHQ-60-X5 with the longest persistence length was 21.76% larger than that of TAHQ-60-X0, indicating that the construction of long persistence lengths can effectively broaden the elastic deformation range of CPI films.

Based on the beneficial effect of long persistence lengths on the elastic deformation range of CPI films, the static folding resistance of CPI films with various persistence lengths was compared according to the method shown in the support information [57,58]. As shown in Fig. 6 (f-i) and Fig. S5, during the folding radius decreased from 3 mm to 1 mm, the folding angle of TAHQ-60-X0 decreased rapidly from 130° to 90°. Other CPI films also showed the same change rule, indicating that as the folding radius decreased, CPI films were more prone to crease damage during folding. In addition, under the same folding radius, such as R = 3 mm, the folding angles of TAHQ-60-X0, TAHQ-60-X1, TAHQ-60-X3 and TAHQ-60-X5 were 130°, 135°, 140° and 142°, respectively, showing a trend of increasing with the increase of elastic deformation range of CPI films, indicating that CPI films with large elastic deformation range had better static folding resistance. Among them, the folding angles of TAHQ-60-X5 with the longest persistence length at 3 mm, 2 mm and 1 mm folding radius were 142°, 132° and 120°, respectively, which were 9.2%, 11.8% and 25% larger than that of TAHQ-60-X0, indicating that the long persistence length of CPI films can significantly improve the static folding resistance of CPI films by broadening the elastic deformation range.

4. Conclusion

In this work, CPI films with various persistence lengths were successfully prepared by controllable polymerization. It was found that with the persistence lengths of CPI films increased from $2.17 \pm 0.07 \text{ \AA}$ to $16.56 \pm 0.12 \text{ \AA}$, the transmittance of CPI films at 550 nm remained above 85%, and the D_f at 10 GHz of CPI films reduced from 0.00479 to 0.00407 with decrease of 15.1%, while D_k at 10 GHz of CPI films remained at a lower level near 3.0. Besides, TAHQ-60-X5 with the longest persistence length of $16.56 \pm 0.12 \text{ \AA}$ also exhibited thermal expansion coefficients of 24.8 ppm/K, tensile strength of 162.5 MPa and Young's moduli of 4.88 GPa, which were 30.1%, 25.8% and 49.7% better than that of TAHQ-60-X0 with the shortest persistence length of $2.17 \pm 0.07 \text{ \AA}$. Furthermore, TAHQ-60-X5 with the longest persistence length of $16.56 \pm 0.12 \text{ \AA}$ also had better folding resistance properties. Therefore, CPI films with excellent transmittance, low dielectric loss at 10 GHz, outstanding thermal and mechanical properties, and excellent folding resistance were prepared by tuning the persistence lengths of CPI films, which exhibited high application prospect.

CRediT authorship contribution statement

Yitian Qin: Writing – original draft, Resources, Methodology, Formal analysis, Data curation. **Qian Yin:** Resources, Methodology, Formal analysis, Data curation. **Junwei Lyu:** Writing – review & editing, Resources, Methodology, Formal analysis. **Xu Wang:** Funding acquisition. **Xiangyang Liu:** Writing – review & editing, Validation, Supervision, Project administration, Funding acquisition, Conceptualization.

Declaration of competing interest

The authors declare that they have no known competing financial interests or personal relationships that could have appeared to influence the work reported in this paper.

Data availability

No data was used for the research described in the article.

Acknowledgements

This work was financially supported by the National Natural Science Foundation of China (Grant Nos.52173008, 52273012). The National Demonstration Center for Experimental Materials Science and Engineering Education of Sichuan University was acknowledged for characterization. The Analytical and Testing Center of Sichuan University was acknowledged for characterization and providing Materials Studio, and we are grateful to Daichuan Ma and Daibing Luo for their help with computational simulations. Shaolan Wang of the Analytical and Testing Center of Sichuan University is also acknowledged for her help with DSC tests and analyses.

Appendix A. Supplementary data

Supplementary data to this article can be found online at <https://doi.org/10.1016/j.polymer.2024.126853>.

References

- [1] J. Xie, D. Jia, M. Dirican, Y. Xia, C. Li, Y. Liu, M. Cui, C. Yan, J. Wan, H. Liu, G. Chen, X. Zhang, J. Tao, Highly foldable, super-sensitive, and transparent nanocellulose/ceramic/polymer cover windows for flexible OLED displays, *ACS Appl. Mater. Interfaces* 14 (14) (2022) 16658–16668.
- [2] J. Chen, Y. Ma, T. Chen, Y. Du, J. Xu, D. Wang, J. Yang, P. Hu, J. Jing, B. Yao, J. Fu, Transparent high-performance supramolecular plastics operating in all-weather environments, *Adv. Funct. Mater.* 33 (11) (2023).
- [3] Y.Y. Liu, Y.K. Wang, D.Y. Wu, Synthetic strategies for highly transparent and colorless polyimide film, *J. Appl. Polym. Sci.* 139 (28) (2022).
- [4] W.-F. Peng, H.-Y. Lei, X.-X. Zhang, L.-H. Qiu, M.-J. Huang, Fluorine substitution effect on the material properties in transparent aromatic polyimides, *Chin. J. Polym. Sci.* 40 (7) (2022) 781–788.
- [5] Y. Liu, Q. Chen, P. Li, Influence of direct fluorination treatment on surface and optical properties of colorless and transparent polyimides, *Mater. Chem. Phys.* (2023) 308.
- [6] H. Min, B. Kang, Y.S. Shin, B. Kim, S.W. Lee, J.H. Cho, Transparent and colorless polyimides containing multiple trifluoromethyl groups as gate insulators for flexible organic transistors with superior electrical stability, *ACS Appl. Mater. Interfaces* 12 (16) (2020) 18739–18747.
- [7] B. Li, Z. Yan, T. Zhang, S. Jiang, K. Wang, D. Wang, Y. Liu, Synthesis and properties of novel colorless and thermostable polyimides containing cross-linkable bulky tetrafluorostyrol pendant group and organosoluble triphenylmethane backbone structure, *J. Polym. Sci.* 58 (17) (2020) 2355–2365.
- [8] D. Li, D. Li, Z. Ke, Q. Gu, K. Xu, C. Chen, G. Qian, G. Liu, Synthesis of colorless polyimides with high T_g and low coefficient of thermal expansion from benzimidazole diamine containing biamide, *J. Polym. Sci.* 61 (9) (2023) 818–828.
- [9] D. Li, C. Wang, X. Yan, S. Ma, R. Lu, G. Qian, H. Zhou, Heat-resistant colorless polyimides from benzimidazole diamines: synthesis and properties, *Polymer* (2022) 254.
- [10] Y. Luo, K. Chen, W. Wang, R. Bei, C. Li, Y. Long, Z. Zhou, S. Liu, Z. Chi, J. Xu, Y. Zhang, Synthesis and characterization of a large Stokes-shifted fluorescent imide and its related polyimides bearing 2-(2'-hydroxyphenyl)benzothiazole moieties, *J. Mater. Chem. C* 11 (27) (2023) 9252–9261.
- [11] X. Hu, H. Mu, Y. Wang, Z. Wang, J. Yan, Colorless polyimides derived from isomeric dicyclohexyl-tetracarboxylic dianhydrides for optoelectronic applications, *Polymer* 134 (2018) 8–19.
- [12] X. Hu, J. Yan, Y. Wang, H. Mu, Z. Wang, H. Cheng, F. Zhao, Z. Wang, Colorless polyimides derived from 2R,5R,7S,10S-naphthanetetracarboxylic dianhydride, *Polym. Chem.* 8 (39) (2017) 6165–6172.
- [13] J. Miao, M. Zhang, Y. Pang, Z. Zheng, C. Tian, Z. Wang, J. Yan, Colorless polyimides derived from norbornyl bis-benzocyclobutene-containing diamines, *Polym. Chem.* 14 (1) (2023) 62–70.
- [14] Z. Lan, C. Li, Y. Yu, J. Wei, Colorless semi-alicyclic copolyimides with high thermal stability and solubility, *Polymers* 11 (8) (2019).
- [15] D. Zhou, L.I. Kong, S.m. Liu, Y.c. Yuan, Y.g. Ma, M.j. Huang, Y.q. Mo, D.h. Qin, J. q. Zhao, Synthesis of novel biphenyl-fused alicyclic tetracarboxylic dianhydride and its performance in thermostable and transparent colorless polyimides, *J. Appl. Polym. Sci.* (2023).
- [16] R. Sawada, S. Ando, Colorless, low dielectric, and optically active semialicyclic polyimides incorporating a biobased isosorbide moiety in the main chain, *Macromolecules* 55 (15) (2022) 6787–6800.
- [17] Y. Zhuang, R. Orita, E. Fujiwara, Y. Zhang, S. Ando, Colorless partially alicyclic polyimides based on tröger's base exhibiting good solubility and dual fluorescence/phosphorescence emission, *Macromolecules* 52 (10) (2019) 3813–3824.
- [18] H. Liu, L. Zhai, L. Bai, M. He, C. Wang, S. Mo, L. Fan, Synthesis and characterization of optically transparent semi-aromatic polyimide films with low fluorine content, *Polymer* 163 (2019) 106–114.

- [19] L. Zhai, S. Yang, L. Fan, Preparation and characterization of highly transparent and colorless semi-aromatic polyimide films derived from alicyclic dianhydride and aromatic diamines, *Polymer* 53 (16) (2012) 3529–3539.
- [20] J. Miao, X. Hu, X. Wang, X. Meng, Z. Wang, J. Yan, Colorless polyimides derived from adamantane-containing diamines, *Polym. Chem.* 11 (37) (2020) 6009–6016.
- [21] Y. Tong, W. Huang, J. Luo, M. Ding, Synthesis and properties of aromatic polyimides derived from 2,2,73,33-biphenyltetracarboxylic dianhydride, *J. Polym. Sci. Polym. Chem.* 37 (10) (1999) 1425–1433.
- [22] M. Zhang, J. Miao, Y. Xu, Z. Wang, J. Yan, Colorless polyimides from fluorinated ladder diamines containing norbornyl benzocyclobutene segments, *Macromolecules* 55 (18) (2022) 7992–8001.
- [23] H. Lei, F. Bao, W. Peng, L. Qiu, B. Zou, M. Huang, Torsion effect of the imide ring on the performance of transparent polyimide films with methyl-substituted phenylenediamine, *Polym. Chem.* 13 (48) (2022) 6606–6613.
- [24] Y.-Y. Liu, J.-H. Cao, Y. Wang, S.-G. Shen, W.-H. Liang, D.-Y. Wu, Colorless polyamide-imide films with enhanced thermal and dimensional stability and their application in flexible OLED devices, *ACS Appl. Polym. Mater.* 4 (10) (2022) 7664–7673.
- [25] Y. Liu, X. Qian, H. Shi, W. Zhou, Y. Cai, W. Li, H. Yao, New poly(amide-imide)s with trifluoromethyl and chloride substituents: synthesis, thermal, dielectric, and optical properties, *Eur. Polym. J.* 94 (2017) 392–404.
- [26] W. Zhang, Q. Wu, W. Shao, F. Li, H. Chen, Y. Pei, J. Wang, Soluble and cross-linkable polyimides from a vanillin-derived diamine: preparation, post-polymerization and properties, *Polym. Chem.* 14 (36) (2023) 4188–4198.
- [27] X. Xia, X. He, S. Zhang, F. Zheng, Q. Lu, Short-side-chain regulation of colorless and transparent polyamide-imides for flexible transparent displays, *Eur. Polym. J.* (2023) 191.
- [28] J. Xing, G. Zhu, X. Fang, G. Chen, Preparation of soluble colorless poly(amide-imide) films with high glass transition temperature and low coefficient of thermal expansion by coordination interaction of Li cations, *J. Polym. Sci.* (2023).
- [29] C. Ahn, T.Y. Kim, P.H. Hong, S. Choi, Y.J. Lee, H. Kwon, H. Jeon, D.W. Ko, I. Park, H. Han, S.W. Hong, Highly transparent, colorless optical film with outstanding mechanical strength and folding reliability using mismatched charge-transfer complex intensification, *Adv. Funct. Mater.* 32 (20) (2022).
- [30] L. Chen, H. Yu, M. Dirican, D. Fang, Y. Tian, C. Yan, J. Xie, D. Jia, H. Liu, J. Wang, F. Tang, X. Zhang, J. Tao, Highly transparent and colorless nanocellulose/polyimide substrates with enhanced thermal and mechanical properties for flexible OLED displays, *Adv. Mater. Interfac.* 7 (20) (2020).
- [31] Q. Yin, Y. Qin, J. Lv, X. Wang, L. Luo, X. Liu, Reducing intermolecular friction work: preparation of polyimide films with ultralow dielectric loss from MHz to THz frequency, *Ind. Eng. Chem. Res.* 61 (49) (2022) 17894–17903.
- [32] A.P. Melissaris, J.A. Mikroyannidis, Thermally stable polymers based on bismaleimides containing amide, imide, and ester linkages, *J. Polym. Sci. Polym. Chem.* 27 (1) (2003) 245–262.
- [33] Q. Yin, Y. Hu, Y. Qin, Z. Cheng, L. Luo, X. Liu, Construction of polyimide films with excellent dimensional stability and toughness via incorporating point-to-face multi-coordination structure, *Compos. B Eng.* (2021) 208.
- [34] I. Butnaru, C.-P. Constantin, M. Asandulesa, A. Wolińska-Grabczyk, A. Jankowski, U. Szeluga, M.-D. Damaceanu, Insights into molecular engineering of membranes based on fluorinated polyimide-polyamide miscible blends which do not obey the trade-off rule, *Separation and Purification Technology* (2020) 233.
- [35] R.G. Pereyra, M.A. Carignano, Molecular dynamics study of polymeric chemical gels: effect of persistence length and crosslinker density, *J. Polym. Sci. B Polym. Phys.* 57 (19) (2019) 1343–1350.
- [36] C. He, A.H. Windle, Persistence lengths of aromatic polyamides: a computer simulation approach, *Macromolecular Theory and Simulations* 4 (2) (2003) 289–304.
- [37] M. Otto, J. Eckert, T.A. Vilgis, Persistence lengths of semiflexible chains — methods and approximations, *Macromolecular Theory and Simulations* 3 (3) (2003) 543–555.
- [38] H.-P. Hsu, W. Paul, K. Binder, Standard definitions of persistence length do not describe the local “intrinsic” stiffness of real polymer chains, *Macromolecules* 43 (6) (2010) 3094–3102.
- [39] J.S. Hernández-Fragoso, S.d.J. Alas, A.G. Goicochea, Polymer chains of a large persistence length in a polymer brush require a lower force to be compressed than chains with a short persistence length, *ACS Appl. Polym. Mater.* 2 (11) (2020) 5006–5013.
- [40] S. Kozuharov, M. Radiom, P. Maroni, M. Borkovec, Persistence length of poly(vinyl amine): quantitative image analysis versus single molecule force response, *Macromolecules* 51 (10) (2018) 3632–3639.
- [41] K.M. Salerno, N. Bernstein, Persistence length, end-to-end distance, and structure of coarse-grained polymers, *J. Chem. Theor. Comput.* 14 (4) (2018) 2219–2229.
- [42] I. Živić, S. Elezović-Hadžić, D. Marčetić, Persistence length of semi-flexible polymer chains on Euclidean lattices, *Phys. Stat. Mech. Appl.* (2022) 607.
- [43] J. F. P., *Statistical Mechanics of Chain Molecules*, Interscience Publishers, New York, 1969.
- [44] M. Ree, K. Kim, S.H. Woo, H. Chang, Structure, chain orientation, and properties in thin films of aromatic polyimides with various chain rigidities, *J. Appl. Phys.* 81 (2) (1997) 698–708.
- [45] P.K. Chakrabarti, T. Nammalvar, R.C. Sastri, Diffusion-coefficient for model potentials through mean-square displacement, *Chem. Phys. Lett.* 71 (2) (1980) 277–279.
- [46] U.O. Uyor, A.P.I. Popoola, O.M. Popoola, V.S. Aigbodion, Advancement on suppression of energy dissipation of percolative polymer nanocomposites: a review on graphene based, *J. Mater. Sci. Mater. Electron.* 30 (18) (2019) 16966–16982.
- [47] G.V. Kuznetsov, E.V. Kravchenko, N.A. Pribatuirin, Dielectric loss in the polymer-semiconductor-composite system with allowance for nonlinear dependence of electric characteristics on temperature resulting from microwave irradiation, *J. Commun. Technol. Electron.* 63 (4) (2018) 381–387.
- [48] Y. Zhang, S. Ke, H. Huang, L. Zhao, L. Yu, H.L.W. Chan, Dielectric relaxation in polyimide nanofoamed films with low dielectric constant, *Appl. Phys. Lett.* 92 (5) (2008).
- [49] C. Li, A. Strachan, Cohesive energy density and solubility parameter evolution during the curing of thermoset, *Polymer* 135 (2018) 162–170.
- [50] M. Lian, X. Lu, Q. Lu, Synthesis of superheat-resistant polyimides with high Tg and low coefficient of thermal expansion by introduction of strong intermolecular interaction, *Macromolecules* 51 (24) (2018) 10127–10135.
- [51] R. Qin, L. Peng, H. Deng, Y. Liu, X. Liu, Enhancing thermal dimensional stability of polyimide composite films through in-situ constructing highly interfacial grafting degree to constrain early chain relaxation, *Compos. B Eng.* (2021) 216.
- [52] Y.-J. Choi, W.-J. Yoon, G. Bang, J. Jeong, J.-H. Lee, N. Kim, K.-U. Jeong, Coatable compensator for flexible display: single-layered negative dispersion retarder fabricated by coating, self-assembling, and polymerizing host-guest reactive mesogens, *ACS Appl. Mater. Interfaces* 11 (19) (2019) 17766–17773.
- [53] Y.-M. Chang, W.-Y. Yeh, P.-C. Chen, Highly foldable transparent conductive films composed of silver nanowire junctions prepared by chemical metal reduction, *Nanotechnology* 25 (28) (2014).
- [54] Z. Zhou, Y. Zhang, S. Liu, Z. Chi, X. Chen, J. Xu, Flexible and highly fluorescent aromatic polyimide: design, synthesis, properties, and mechanism, *J. Mater. Chem. C* 4 (44) (2016) 10509–10517.
- [55] K. Kim, J. Kim, B.G. Hyun, S. Ji, S.-Y. Kim, S. Kim, B.W. An, J.-U. Park, Stretchable and transparent electrodes based on in-plane structures, *Nanoscale* 7 (35) (2015) 14577–14594.
- [56] Q. Yin, X. Li, Y. Qin, K. Fan, X. Wang, X. Liu, Fabrication of ultralarge curvature folding-resistant polyimide films by widening the elastic range and intermolecular slippery spacing, *Macromolecules* 56 (11) (2023) 4362–4370.
- [57] G. Chen, K.-M. Chang, K.-T. Chen, H.-Y. Chen, C.-J. Lee, J.-C. Ho, J.-L. Chen, C.-C. Lee, 46-1: invited paper: high impact resistance out-fold touch AMOLED display module, *SID Symposium Digest of Technical Papers* 50 (1) (2019) 628–631.
- [58] P.H. Gu, S. Du, C.Y. Xie, B.M. Cai, S. Zhang, Y.X. Shi, 74-2: the excellent mechanical properties of novel polymer film and its application in the foldable AMOLED displays, *SID Symposium Digest of Technical Papers* 50 (1) (2019) 1056–1059.